ACS Photonics

Letter

pubs.acs.org/journal/apchd5

Radio Frequency Electromechanical Control over a Surface Plasmon Polariton Coupler

Claudia Ruppert,*[,†] Frederike Förster,[†] Artur Zrenner,[‡] Jörg B. Kinzel,[§,∥,⊥] Achim Wixforth,[§,∥,⊥] Hubert J. Krenner,[§,∥,⊥] and Markus Betz[†]

[†]Experimentelle Physik 2, Technische Universität Dortmund, Germany

[‡]Department Physik, Universität Paderborn, Germany

[§]Lehrstuhl für Experimentalphysik 1, Augsburg Centre for Innovative Technologies (ACIT), Universität Augsburg, Germany

[∥]Center for Nanoscience (CeNS), Ludwig-Maximilians-Universität München, München, Germany

[⊥]Nanosystems Initiative Munich, Schellingstr. 4, 80799 München, Germany

ABSTRACT: We explore the impact of ∼500 MHz surface acoustic waves traveling across a commensurable plasmonic grating coupler. A stroboscopic technique involving surface acoustic waves synchronized to a modelocked optical source allows to time-resolve the dynamical impact of the electromechanically induced perturbation. The surface acoustic wave periodically enhances or decreases the surface ripple of the static grating. Most remarkably, the dynamic surface deformation deliberately modulates the coupler's efficiency by ±2% during the ∼2 ns acoustic cycle.

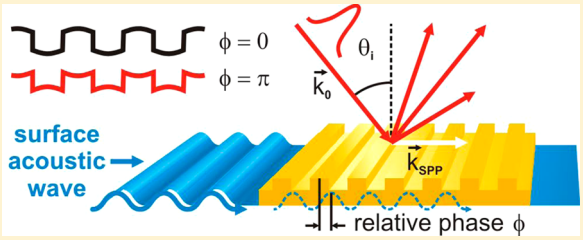

KEYWORDS: *plasmonics, nanomechanics, surface acoustic waves, surface plasmon polaritons*

Surface plasmon polaritons (SPPs) are key to next-generation nanophotonics.[1,2] Efficient conversion of free-space radiation into these surface-bound electromagnetic modes is routinely achieved via patterned metal films. The emerging field of "active plasmonics",[3] however, aims for control-on-demand over the generation and evolution of guided SPPs. So far, interesting strategies for all-optical switching of SPP launching and propagation have been realized which provide THz modulation bandwidth.[4−6] However, these approaches are hampered by the large irradiances required. In contrast, substantial high-frequency mechanical distortions can be easily driven all-electrically using conventional radio frequency (RF) electronics. Such hypersound waves have already found diverse applications in semiconductor nanophotonics.[7,8] Here we explore the impact of ∼500 MHz surface acoustic waves (SAWs) traveling across a commensurable, static gold grating, that is, a paradigm for a SPP injector. In essence, the electromechanically induced, dynamic surface deformation deliberately modulates the launcher's coupling characteristics on subnanosecond time scales as required for device applications.

The dispersion relation of SPPs on a metal surface is characterized by a pronounced wave-vector mismatch with respect to light in vacuum. As a result, direct optical excitation of SPPs on a planar surface is inhibited. In turn, this mode mismatch also prohibits SPPs from reradiating into free space and, thereby, ensures robust SPP propagation over distances of many μm. The most viable concepts for the controlled launch of SPPs utilize dielectric prisms or patterned surfaces. Among these different approaches, spatially periodic surface gratings are probably the most direct tool to overcome the wave-vector mismatch and to achieve efficient and broadband conversion of light into SPPs. However, they are intrinsically static and therefore lack fast tunability, an aspect incompatible with the requirements of modern high-speed nanophotonics. The guiding idea of the present work is to realize a grating based SPP coupler with dynamically tunable, electromechanically controlled coupling characteristics. To this end, we implement gold microstructures combining a static surface-relief grating with dynamic, propagating SAWs of the same spatial periodicity. Depending on the exact timing of the all-electrically generated SAW, those two commensurable surface deformations interfere constructively or destructively and, thereby, yield a fast modulation of the SPP coupling efficiency. Most remarkably, we will demonstrate below that our present technique favorably combines the convenience of RF electrical control over a SPP launcher with an efficient modulation with GHz bandwidth. Our approach has conceptual similarities to previous experiments involving the photoexcitation of predefined gratings[6,9] or the creation of dielectric gratings by interference of laser pulses.[10,11] In our own previous work, we have identified a minute launching mechanism for SPPs related to the surface profile of SAWs only.[12] However, all those mechanisms either require large optical irradiances or only permit a weak influence on the conversion between light and SPPs.

Received: September 3, 2013
Published: January 31, 2014

   dx.doi.org/10.1021/ph400022u | *ACS Photonics* 2014, 1, 91−95

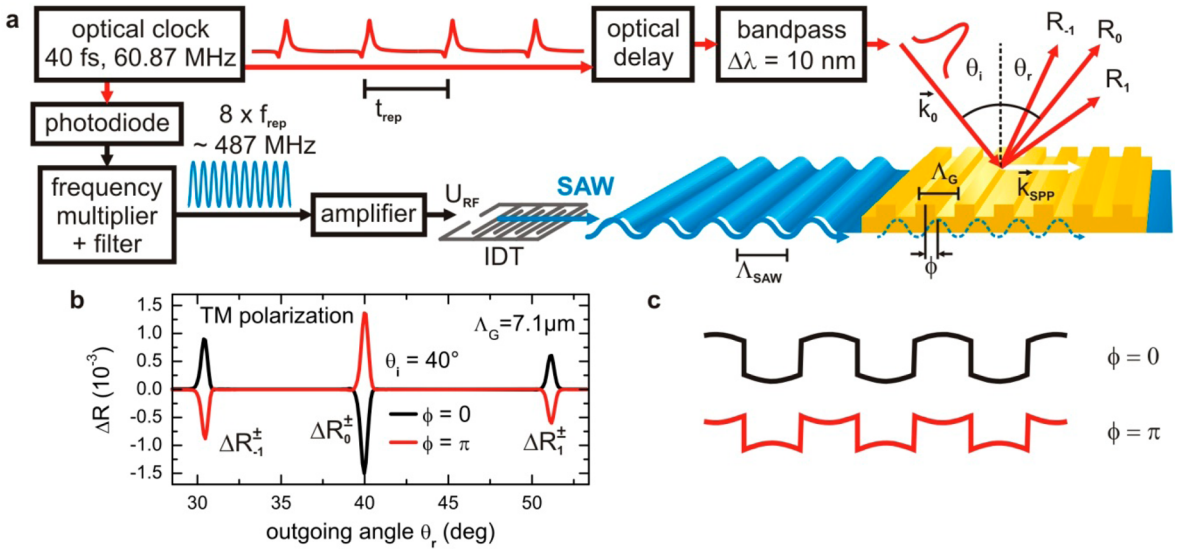

Figure 1. Experimental setup and sample characteristics. (a) Schematic of the experiment: A mode-locked Ti:sapphire laser serves as an optical source and as a clock. The 8th harmonic of the laser repetition rate is generated electronically and fed to IDTs on the $LiNbO_3$ chip. It induces a SAW synchronized to the optical pulse train. This SAW modulates the surface profile of a rectangular gold grating formed on the $LiNbO_3$. The optical delay sets the relative phase between the RF wave and the near-infrared pulse train and, thus, permits to optically interrogate the device at a fixed spatial phase difference ϕ between the static grating and the dynamic surface deformation of the SAW. (b) SAW-induced changes of the grating's TM reflectivity (ΔR_0 observed at $\theta_r = \theta_i$) and first order diffraction ($\Delta R_{\pm 1}$) for light incident at $\theta_i = 40°$ far away from the SPP resonance angle. The black (red) line corresponds to results for $\phi = 0$ ($\phi = \pi$). The RF power is $P_{RF} = 20.5$ dBm. (c) Schematic rendering of the SAW impact on the surface relief for those phases (not to scale).

The samples are fabricated by standard e-beam lithography in a lift-off process on chemically reduced ("black") $LiNbO_3$. The crystal orientation is 128° YX-cut so that only Rayleigh-type waves are induced at the $LiNbO_3$ surface leading to an approximately sinusoidal periodic deformation perpendicular to the surface by the SAW. The electrodes for the SAW excitation, so-called interdigital transducers (IDTs), consist of 54 pairs of single-electrode fingers of 60 nm height and ~1.5 μm width formed from aluminum on top of a 10 nm titanium adhesion layer. The spacing of adjacent electrodes is 4 μm and the applied voltage alternates in sign between neighboring electrodes. By applying a RF signal of ~487 MHz, a SAW of ~8 μm wavelength is launched via to the inverse piezoelectric effect. Due to short circuiting and mass loading, the SAW velocity underneath the metalized area is reduced so that the actual SAW wavelength modulating the grating is practically identical to $\Lambda_G = 7.1$ μm. The maximum RF power levels fed to the IDTs is ~20 dBm. We use two IDT structures with a separation of ~2.5 mm in delay line geometry in order to also monitor the transmitted RF power and to determine the IDTs' resonance frequency. The gold gratings are deposited in the center area between the two IDTs. They are grown in a three-step process beginning with a 10 nm titanium adhesion layer. Then 42 gold slabs of 50 nm height, ~4 μm width, and Λ_G = 7.1 μm spacing are deposited. These are finally then overgrown with a 100 nm thick gold film creating a grating of 250 μm × 300 μm lateral dimension, 7.1 μm grating period, and 50 nm groove depth.

For optical spectroscopy of the dynamical impact of SAWs on the plasmonic device, the SAW has to be synchronized with an optical source. Similar stroboscopic concepts to phase-lock SAWs or RF electrical signals to optical pulse trains have already been successfully employed to control and probe various semiconductor nanostructures.[7,13,14] Figure 1a shows the schematic of our experiment. A mode-locked Ti:sapphire laser optimized for long-wavelength operation[15] produces a train of 40 fs pulses at a central wavelength of 940 nm. Its repetition rate is continuously adjustable since the output coupler is mounted on a translation stage. The repetition rate f_{rep} of this optical clock is deliberately set to $f_{rep} = 60.872$ MHz. A portion is detected with a fast photodiode. It is connected to an electronic frequency multiplier while a RF filter selects the eighth harmonic at $f_{SAW} = 8f_{ref} = 486.98$ MHz. This frequency component is amplified and fed into the IDTs, thereby generating a SAW automatically locked to the optical pulse train. Another portion of the near-infrared pulse train is passed through a delay line to precisely set its arrival to a well-defined time within the acoustic cycle of the SAW. A filter of 10 nm bandwidth selects a spectral window around 960 nm. The sample is placed in a θ–2θ rotation stage, while the near-infrared light is loosely focused onto the grating by a f = 150 mm lens with a variable angle of incidence θ_i. The laser spot size is ~200 μm in diameter, with an angular aperture of $\Delta\theta \approx 0.7°$, which determines the angular resolution of our setup. Optical signals are detected as a function of the outgoing angle θ_r. Most of the data is recorded directly in reflection geometry $\theta_r = \theta_i$. The SAW-induced changes of the optical properties are detected using a standard lock-in technique with an ~1.3 kHz amplitude modulation of the RF signal generating the SAW. The values finally given for ΔR_0 and $\Delta R_1^{\pm}$ throughout the paper represent SAW-induced modifications normalized to the reflected light intensity R_0.

We start the optical characterization by addressing how the device acts as a tunable regular diffraction grating and apply a RF power of $P_{RF} \approx 20$ dBm to the IDTs. This part also serves to calibrate the phase of our stroboscopic technique and to determine the SAW amplitude. Note that the RF power levels indicated throughout the paper are externally applied ones. The actual power converted into SAWs is much lower since little effort is made to optimize the electro-mechanical conversion

dx.doi.org/10.1021/ph400022u | ACS Photonics 2014, 1, 91–95

efficiency. Figure 1b shows the SAW induced change of the optical intensity as a function of the outgoing angle θ_r, while the angle of incidence is fixed to $\theta_i = 40°$ (for this incident angle no coupling into SPPs occurs). It contains information about the change of the reflectivity (ΔR_0) and the modifications of the two first-order diffractions (ΔR_1,ΔR_{-1}). The first order diffraction efficiency of the unperturbed grating is 1.5%, while higher order diffraction is more than an order of magnitude smaller. This is also reflected by the SAW-induced modifications where the amplitude of ΔR_0 is roughly the sum of the first order diffraction changes. It is reasonable to assume that maximum changes of both the reflectivity and the diffraction efficiency occur when the SAW on average increase ($\phi = 0$) or decrease ($\phi = \pi$) the predefined grooves (cf. schematic in Figure 1c). Changing the delay between the optical pulse train and the SAW by half an acoustic cycle ($\Delta t = T_{SAW}/2 \approx 1$ ns) induces a phase shift of $\Delta\phi = \pi$ and, correspondingly, causes a complete reversal of the reflectivity and diffraction signatures in Figure 1b. From the signal magnitudes in Figure 1b and a simple model neglecting the details of the surface profile, we can extract the out-of-plane amplitude of the SAW. We assume that the first-order diffraction efficiency R_1 scales quadratically with the groove depth d. This scaling has been derived analytically for a sinusoidal grating profile with small amplitude ($d \ll \Lambda_G$)[16] and is also consistent with simulations for other shallow surface reliefs.[17] Therefore, $R_1^{\pm} \propto (d \pm \delta)^2$ with the SAW peak-to-peak amplitude δ that increases ($\phi = 0$) or diminishes ($\phi = \pi$) the groove depth of the static grating. The detected signal is the difference of the diffraction efficiency with and without the SAW, that is, $\Delta R_1^{+} \propto \delta^2 + 2\delta d$ ($\Delta R_1^{-} \propto \delta^2 + 2\delta d$)^2 for $\phi = 0$ ($\phi = \pi$). For $\delta \ll d$, the relative diffractivity change is $\Delta R_1^{\pm}/R_1 \approx \pm 2\delta/d$. For the present device, with $R_1 = 1.5\%$, we find a SAW-induced change of $\Delta R_1^{\pm} = 6.2 \times 10^{-4}$ at $\phi = 0$. With a groove depth of $d = 50$ nm, this yields a realistic SAW amplitude of $\delta \approx 1$ nm, comparable to previous measurements on similar IDT structures on $LiNbO_3$.[12]

The operational principle of a plasmonic grating coupler is straightforward. Any spatial pattern of periodicity Λ_G can provide an additional momentum $K_G = 2\pi/\Lambda_G$ to overcome the mismatch between the wavevectors k_{SPP} of the SPP and $k_0 = \omega/c$ of light in vacuum. Once fulfilling the condition $k_{SPP} = k_0 \sin(\theta_i) \pm mK_G$, with an integer m, light with an off-normal angle of incidence θ_i, and a polarization parallel to the plane of incidence (transverse magnetic, TM) couples resonantly to SPPs. As plausible from the well-known dielectric properties of gold, the present grating permits light of 960 nm wavelength to resonantly launch SPPs at an angle of $\theta_i = 61.7°$ and $m = 1$. To determine the actual SPP coupling for the unperturbed device, we measure the angular dependence of its reflectivity ($R_0(\theta_i)$). The data for transverse electric (TE) polarization in Figure 2a only show an unpronounced angular dependence. In marked contrast, the reflectivity for TM polarized light shows a prominent dip close to the theoretically expected SPP resonance angle. A Lorentzian fit to the data reveals a resonance angle $\theta_i = 61.8°$ with a resonant conversion efficiency for light into SPPs of $A_{SPP} = 0.09$.

We now turn toward the central aspect of this study, which is the change of the SPP resonance when superimposing the dynamic grating of the SAW. First, we determine the time-averaged SAW-induced changes for a RF signal not locked to the optical source. Figure 2b shows the corresponding SAW-induced changes of the TM reflectivity. It is characterized by an

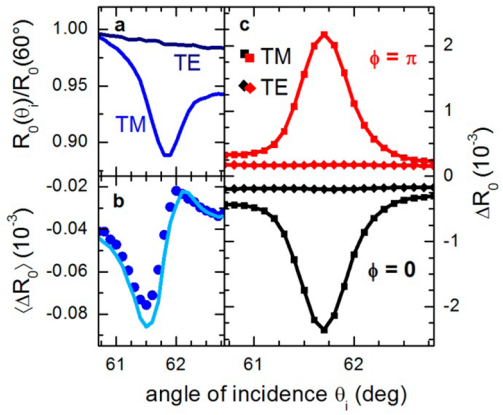

Figure 2. SAW-induced changes of the reflectivity for TM and TE polarized light. (a) Reflectivity of the unperturbed gold grating close to the SPP resonance at $\theta_i = 61.7°$. (b) Solid circles: Angular dependence of the SAW-induced reflectivity changes for TM polarized light obtained with an unsynchronized SAW. The solid line shows the ϕ-averaged results of the phase-dependent data in Figure 3 as a comparison. (c) Corresponding TM and TE data for $\phi = 0$ and π once the SAW is locked to the optical pulse train. The RF power in panels (b) and (c) is $P_{RF} = 20.5$ dBm.

induced absorption with an amplitude of $\Delta R_0 \approx 4 \times 10^{-5}$ close to the SPP resonance angle $\theta_i = 61.7°$. In marked contrast, we observe much larger and richer signatures once ϕ is fixed via the described stroboscopic technique. Figure 2c displays the angular dependence of the SAW-induced reflectivity changes for $\phi = 0$ and $\phi = \pi$. The TE data only show a θ_i-independent offset related to the ϕ-dependent changes of the diffraction efficiency. More importantly, the TM results reveal pronounced signals at the SPP resonance with magnitudes as large as $\Delta R_0 \approx \pm 2 \times 10^{-3}$. When combined with the data of the unperturbed grating in Figure 2a, they are indicative of a SAW-related change of the efficiency of the SPP launcher as large as $\Delta R_{0,max}/A_{SPP} \approx \pm 2\%$, that is, a similar modulation depth, as seen for the diffraction efficiency. We note that this modulation amplitude for SPP launching is also similar to that of recent all-optical approaches[5,6] that, however, require the use of sophisticated pulsed laser sources instead of the present all-electrical concept.

Further details of the SAW impact on the device are revealed by systematically studying the SAW-induced reflectivity changes as a function of the phase ϕ. Figure 3 shows such ΔR_0 data for various angles θ_i close to the SPP resonance angle and TM polarized light. For all θ_i we find a background signal that scales $\propto\cos(\phi)$ and has only an unpronounced angular dependence. It originates from the enhancement or suppression of the grating's diffraction induced by the SAW. In marked contrast, we see much larger ΔR_0 around the SPP resonance angle with peak signals of $\Delta R_0 \approx \pm 2 \times 10^{-3}$, as already seen in Figure 2c, where we show horizontal cuts of this 2D representation along $\phi = 0$ and π. Remarkably, the angular dependences also contain dispersive features around $\theta_i = 61.7°$, which are most prominent at $\phi = \pm\pi/2$. These signatures arise from a slight mismatch between Λ_G and Λ_{SAW}. We want to emphasize that the ϕ-axis corresponds to a real time. In particular, the time delay between the maximum enhancement or suppression of the SPP coupling efficiency is as short as $\Delta t = T_{SAW}/2 \approx 1$ ns. From Figure 3 we also extract ϕ-averaged reflectivity changes ΔR_0, which are shown as a solid line in Figure 2b. They agree very well with the findings for the SAW-induced modifications obtained with an unsynchronized RF

dx.doi.org/10.1021/ph400022u | ACS Photonics 2014, 1, 91−95

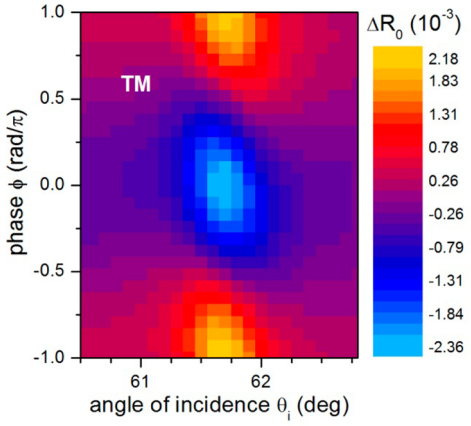

Figure 3. Phase-dependent, SAW-induced reflectivity changes (ΔR_0) for TM polarized light. The 2D representation summarizes results for various angles θ_i and relative phases ϕ between the traveling SAW and the static grating.

source. Those remaining signal contributions can also be explained by the above model, where the grating's diffraction efficiency and SPP coupling scales $\propto(d \pm \delta)^2$. When computing such modifications for the present $\delta \propto \cos\phi$ situation, the ϕ-averaged relative change to the SPP coupling efficiency is related to the previously neglected δ^2-term and is expected to be $\delta^2/(2d^2) \approx 2 \times 10^{-4}$, in fair agreement with the observed $\langle \Delta R_0 \rangle / A_{SPP} \approx 4 \times 10^{-4}$.

To further support our findings, we measure ΔR_0 for various RF powers. Here we utilize the second IDT in delay line geometry to analyze the acoustic power in the device. For elevated RF powers we find the temperature of the sample to increase and, therefore, the IDT's resonance frequency to slightly shift so that the transmitted RF power is a more reliable measure of the SAW amplitude. Figure 4 displays the reflectivity change for TM polarization detected at the SPP resonance for $\phi = 0$ and π. Angular scans for three exemplary power levels are shown in panel (a). The peak signals ΔR_{SPP} of the SPP resonance amplitude are then plotted as a function of to the RF power P_{RF} (cf. Figure 4b) with the maximum value

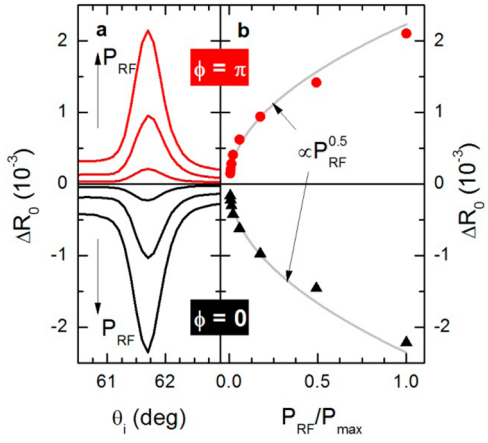

Figure 4. Dependence on the RF power. (a) Angular dependence of the SAW-induced TM reflectivity changes (ΔR_0) for three exemplary RF powers. The black (red) line corresponds to $\phi = 0$. (b) Symbols: Power dependence of the SAW-induced modification of the SPP coupling efficiency for various RF powers normalized to $P_{max} = 20.5$ dBm. The solid lines represent a scaling $\Delta R_0 \propto (P_{RF})^{1/2}$.

corresponding to an overall incident power level of $P_{RF} = 20.5$ dBm. As evident from the solid lines, the data point toward a scaling of $\Delta R_{SPP} \propto P_{RF}{}^{0.5}$. This finding is again in line with the simple model of a SPP launching efficiency $\propto(d \pm \delta)^2$. In particular, the maximum SAW-induced change to the SPP resonance is expected to be $\Delta R_{SPP} \approx \pm 2\delta/d$. For the SAW amplitude δ we know that $\delta \propto (P_{RF})^{1/2}$ so that the model predicts $\Delta R_{SPP} \propto (P_{RF})^{1/2}$, as seen in the experiment.

Finally we want to comment on the scalability and the prospects of the present approach. While the SAW impact reported here is already significant, certain device applications probably require larger modulation depths. There is room to enhance the electromechanical coupling by optimized IDT design. The SAW amplitude δ could be further enlarged to a few nm, only limited by the mechanical stability of the substrate. Moreover, there have been suggestions and reports on shallow surface relief gratings with very efficient SPP coupling.[18,19] These promise that for technologically accessible values of δ/d the absolute modulation of the SPP coupling efficiency can be largely enhanced. In addition, recent theoretical work predicts that, due to an interference of excitation channels, a SAW of wavelength $\Lambda_G/2$ traveling across a permanent grating of periodicity Λ_G can cause drastic modulations of the SPP launching efficiency.[20] The modulation speed itself is governed by the speed of sound. Therefore, we expect the use of SAW frequencies $\lesssim$5 GHz to be within reach by scaling the grating period down to $\sim$1 μm.

AUTHOR INFORMATION

Corresponding Author

*E-mail: claudia.ruppert@tu-dortmund.de.

Notes

The authors declare no competing financial interest.

ACKNOWLEDGMENTS

The work is supported by the DFG in the frameworks of the priority program SPP 1391 "Ultrafast Nanooptics" and the Emmy Noether program (H.J.K.).

REFERENCES

(1) Atwater, H. A. The Promise of Plasmonics. *Sci. Am.* **2007**, *296* (4), 56−62.

(2) Ozbay, E. Plasmonics: Merging Photonics and Electronics at Nanoscale Dimensions. *Science* **2006**, *311* (5758), 189−193.

(3) Krasavin, A. V.; Zheludev, N. I. Active Plasmonics: Controlling Signals in Au/Ga Waveguide Using Nanoscale Structural Transformations. *Appl. Phys. Lett.* **2004**, *84* (8), 1416−1418.

(4) Pacifici, D.; Lezec, H. J.; Atwater, H. A. All-Optical Modulation by Plasmonic Excitation of CdSe Quantum Dots. *Nat. Photonics* **2007**, *1* (7), 402−406.

(5) MacDonald, K. F.; Samson, Z. L.; Stockman, M. I.; Zheludev, N. I. Ultrafast Active Plasmonics. *Nat. Photonics* **2009**, *3* (1), 55−58.

(6) Rotenberg, N.; Betz, M.; van Driel, H. M. Ultrafast Control of Grating-Assisted Light Coupling to Surface Plasmons. *Opt. Lett.* **2008**, *33* (18), 2137−2139.

(7) Fuhrmann, D. A.; Thon, S. M.; Kim, H.; Bouwmeester, D.; Petroff, P. M.; Wixforth, A.; Krenner, H. J. Dynamic Modulation of Photonic Crystal Nanocavities Using Gigahertz Acoustic Phonons. *Nat. Photonics* **2011**, *5* (10), 605−609.

(8) Brüggemann, C.; Akimov, A. V.; Scherbakov, A. V.; Bombeck, M.; Schneider, C.; Höfling, S.; Forchel, A.; Yakovlev, D. R.; Bayer, M. Laser Mode Feeding by Shaking Quantum Dots in a Planar Microcavity. *Nat. Photonics* **2012**, *6* (1), 30−34.

(9) Pohl, M.; Belotelov, V. I.; Akimov, I. A.; Kasture, S.; Vengurlekar, A. S.; Gopal, A. V.; Zvezdin, A. K.; Yakovlev, D. R.; Bayer, M.

Plasmonic Crystals for Ultrafast Nanophotonics: Optical Switching of Surface Plasmon Polaritons. *Phys. Rev. B* **2012**, *85* (8), 081401.
(10) Renger, J.; Quidant, R.; Hulst, N.; van Palomba, S.; Novotny, L. Free-Space Excitation of Propagating Surface Plasmon Polaritons by Nonlinear Four-Wave Mixing. *Phys. Rev. Lett.* **2009**, *103* (26), 266802.
(11) Rotenberg, N.; Betz, M.; van Driel, H. M. Ultrafast All-Optical Coupling of Light to Surface Plasmon Polaritons on Plain Metal Surfaces. *Phys. Rev. Lett.* **2010**, *105* (1), 017402.
(12) Ruppert, C.; Neumann, J.; Kinzel, J. B.; Krenner, H. J.; Wixforth, A.; Betz, M. Surface Acoustic Wave Mediated Coupling of Free-Space Radiation into Surface Plasmon Polaritons on Plain Metal Films. *Phys. Rev. B* **2010**, *82* (8), 081416.
(13) Sauer, W.; Streibl, M.; Metzger, T. H.; Haubrich, A. G. C.; Manus, S.; Wixforth, A.; Peisl, J.; Mazuelas, A.; Härtwig, J.; Baruchel, J. X-Ray Imaging and Diffraction from Surface Phonons on GaAs. *Appl. Phys. Lett.* **1999**, *75* (12), 1709−1711.
(14) Vasconcellos, S. M.; de Gordon, S.; Bichler, M.; Meier, T.; Zrenner, A. Coherent Control of a Single Exciton Qubit by Optoelectronic Manipulation. *Nat. Photonics* **2010**, *4* (8), 545−548.
(15) Ruppert, C.; Betz, M. Generation of 30 fs, 900−970 nm Pulses from a Ti:sapphire Laser Far off the Gain Peak. *Opt. Express* **2008**, *16* (8), 5572−5576.
(16) Raether, H. *Surface Plasmons on Smooth and Rough Surfaces and on Gratings*; Springer: Berlin, 1988.
(17) Moharam, M. G.; Gaylord, T. K. Diffraction Analysis of Dielectric Surface-Relief Gratings. *J. Opt. Soc. Am.* **1982**, *72* (10), 1385−1392.
(18) Rotenberg, N.; Sipe, J. E. Analytic Model of Plasmonic Coupling: Surface Relief Gratings. *Phys. Rev. B* **2011**, *83* (4), 045416.
(19) Koev, S. T.; Agrawal, A.; Lezec, H. J.; Aksyuk, V. A. An Efficient Large-Area Grating Coupler for Surface Plasmon Polaritons. *Plasmonics* **2012**, *7* (2), 269−277.
(20) Rotenberg, N.; Beggs, D. M.; Sipe, J. E.; Kuipers, L. Resonant Coupling from a New Angle: Coherent Control through Geometry. *Opt. Express* **2013**, *21* (14), 16504−16513.